

Charmonium absorption by nucleons

A. Sibirtsev,¹ K. Tsushima,² and A. W. Thomas²

¹*Institut für Theoretische Physik, Universität Giessen, D-35392 Giessen, Germany*

²*Special Research Center for the Subatomic Structure of Matter (CSSM) and Department of Physics and Mathematical Physics, University of Adelaide, Adelaide SA 5005, Australia*

(Received 22 May 2000; published 19 March 2001)

J/Ψ dissociation in collisions with nucleons is studied within a boson-exchange model and the energy dependence of the dissociation cross section is calculated from the threshold for $\Lambda_c \bar{D}$ production to high energies. We illustrate the agreement of our results with calculations based on short-distance QCD and Regge theory. The compatibility between our calculations and the data on J/Ψ photoproduction on a nucleon is discussed. We evaluate the elastic $J/\Psi + N$ cross section using a dispersion relation and demonstrate the overall agreement with the predictions from QCD sum rules. Our results are compatible with the phenomenological dissociation cross section evaluated from the experimental data on J/Ψ production from $\gamma + A$, $p + A$, and $A + A$ collisions.

DOI: 10.1103/PhysRevC.63.044906

PACS number(s): 24.85.+p, 12.38.Mh, 25.20.Lj

I. INTRODUCTION

Very recently the NA50 Collaboration reported [1] measurements of J/Ψ suppression in Pb+Pb collisions at the CERN-SPS. It was claimed in Ref. [1] that these new experimental data ruled out conventional hadronic models of J/Ψ suppression and thus indicated the formation of a deconfined state of quarks and gluons, namely the quark-gluon plasma (QGP). Presently, there are calculations [2–4] using two different methods, namely the cascade [5,6] and the Glauber-type model [7], that reproduce the new NA50 data reasonably well up to the highest transverse energies [1] based on hadronic J/Ψ dissociation alone. In view of this, the evidence for QGP formation based on anomalous J/Ψ suppression [8] is not obvious, and an interpretation of the NA50 data can be further considered in terms of the hadronic dissociation of the J/Ψ meson by the nucleons and comovers.

However, the long term puzzle of the problem is the strength of the hadronic dissociation of the J/Ψ meson. The various calculations [2,3,5–7,9,10] of J/Ψ production from heavy ion collisions in practice adopt different dissociation cross sections. For instance, the cross section for $J/\Psi + N$ dissociation used in these models ranges from 3.0 to 6.7 mb when dealing with the same experimental data on J/Ψ production from $A + A$ collisions. Moreover, it is presently accepted that the dissociation cross section does not depend on the J/Ψ energy, and in the available calculations [2,3,5–7,9,10] it enters as a constant. Furthermore, to a certain extent, both of the cross sections for J/Ψ dissociation on nucleons and comovers were taken as free parameters, finally adjusted to the heavy ion data.

Moreover, the $J/\Psi + N$ cross section was evaluated from experimental data on J/Ψ meson production in $\gamma + A$ and $p + A$ reactions. The analysis of the J/Ψ photoproduction from nuclei at a mean photon energy of 17 GeV [11] indicates a $J/\Psi + N$ cross section of 3.5 ± 0.9 mb. The combined analysis [12] of experimental data on J/Ψ production from $p + A$ collisions at beam energies from 200 to 800 GeV provides a $J/\Psi + N$ cross section of 7.3 ± 0.6 mb. On the other

hand, the $J/\Psi + N$ cross section evaluated by the vector-dominance model from the $\gamma + N \rightarrow J/\Psi + N$ data is about 1 mb [13] for J/Ψ energies in the nucleon rest frame from 8 to 250 GeV.

In principle, this ambiguity in the J/Ψ dissociation cross section does not allow one to claim a consistent interpretation of the NA50 results. Although the experimental data might be well reproduced by the more recent calculations [2–4] considering the hadronic dissociation of the J/Ψ meson, the $J/\Psi + N$ cross section was introduced therein as a free parameter. In Ref. [4] we provided results for J/Ψ dissociation on comovers and motivated the large rate of this process [2,3] as arising from the in-medium modification of the dissociation amplitude, which is obviously different from that given in free space [14,15]. Most recent results from the different models on J/Ψ dissociation on light hadrons are given in Refs. [16–19]. In the present study we apply the hadronic model to $J/\Psi + N$ dissociation.

II. LAGRANGIAN DENSITIES, COUPLING CONSTANTS, AND FORM FACTORS

Within the boson-exchange model we consider the reactions depicted in Fig. 1 and use the interaction Lagrangian densities:

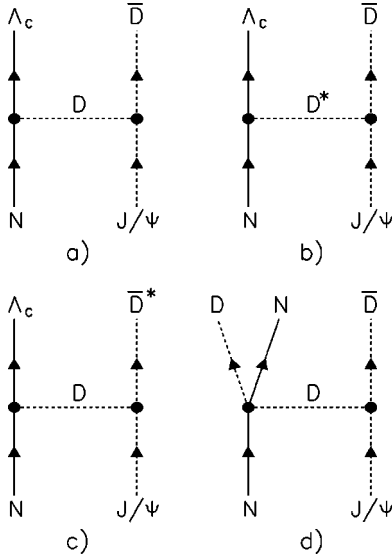
$$\mathcal{L}_{JDD} = ig_{JDD} J^\mu [\bar{D}(\partial_\mu D) - (\partial_\mu \bar{D})D], \quad (1)$$

$$\mathcal{L}_{D\Lambda_c} = ig_{D\Lambda_c} (\bar{N} \gamma_5 \Lambda_c D + \bar{D} \bar{\Lambda}_c \gamma_5 N), \quad (2)$$

$$\mathcal{L}_{JD^*D} = \frac{g_{JD^*D}}{m_J} \varepsilon_{\alpha\beta\mu\nu} (\partial^\alpha J^\beta) [(\partial^\mu \bar{D}^{*\nu})D + \bar{D}(\partial^\mu D^{*\nu})], \quad (3)$$

$$\mathcal{L}_{D^*\Lambda_c} = -g_{D^*\Lambda_c} (\bar{N} \gamma_\mu \Lambda_c D^{*\mu} + \bar{D}^{*\mu} \bar{\Lambda}_c \gamma_\mu N), \quad (4)$$

where,


FIG. 1. The hadronic diagrams for $J/\Psi + N$ dissociation.

$$N = \begin{pmatrix} p \\ n \end{pmatrix}, \quad \bar{N} = N^\dagger \gamma_0, \quad D \equiv \begin{pmatrix} D^0 \\ D^+ \end{pmatrix}$$

(creation of the meson states), $\bar{D} = D^\dagger$, and similar notations for the D^* and \bar{D}^* should be understood.

The JDD coupling constant was derived in Refs. [14,20], and in the following calculations we adopt $g_{JDD} = 7.64$. Following the SU(4) relations from Ref. [21], the $DN\Lambda_c$ coupling constant was taken equal the $KN\Lambda$ coupling constant. The analysis [22–26] of experimental data provides $13.2 \leq g_{KN\Lambda} \leq 15.7$ and in the following we use $g_{DN\Lambda_c} = 14.8$. However, we notice that the calculations [27] by the QCD sum rules suggest a smaller coupling $g_{DN\Lambda_c} \simeq 6.7 \pm 2.1$. The $D^*N\Lambda_c$ coupling constant might be again related to the $K^*N\Lambda$ constant. The $K^*N\Lambda$ constant is given in Ref. [28] within the range $-18.8 \leq g_{K^*N\Lambda} \leq -21.4$, while it varies between $\simeq -5.9$ and -22 in Ref. [29]. In the following calculations, we adopt $g_{D^*N\Lambda_c} = -19$ [28]. Furthermore, we assume that $g_{JDD} = g_{JDD^*}$ [20].

The form factors associated with the interaction vertices were parametrized in a conventional monopole form

$$F(t) = \frac{\Lambda^2}{\Lambda^2 - t}, \quad (5)$$

where t is the four-momentum transfer and Λ is the cutoff parameter. The introduction of the form factors is dictated by the extended structure of the hadrons [30]. The form factor may be estimated through the vector-dominance model (VDM) [31]. The VDM predicts an increase of the form factor with increasing mass of the vector meson and a purely phenomenological prediction provides $\Lambda = m_J$. In the following, we will explicitly use the cutoff parameter $\Lambda = 3.1$ GeV for the form factors at the JDD and JDD^* vertices.

Furthermore, one should also introduce form factors at the $DN\Lambda_c$ and $D^*N\Lambda_c$ vertices. Again, we use the monopole

form but there are no direct ways to evaluate the relevant cutoff parameter. In Refs. [30,32,33] the cutoff parameters were adjusted to fit the empirical nucleon-nucleon data and range from 1.3 to 2 GeV depending on the exchange meson coupled to the NN system. Based on these results, in the following we use a monopole form factor with $\Lambda = 2$ GeV for the $DN\Lambda_c$ and $D^*N\Lambda_c$ vertices.

In principle, the coupling constants and the cutoff parameters in the form factors discussed in this section can be adjusted to the experimental data on the total $J/\Psi + N$ cross section evaluated from different nuclear reactions, as $\gamma + A \rightarrow J/\Psi + X$ and $p + A \rightarrow J/\Psi + X$. On the other hand, these parameters can also be fixed by comparison to the short range QCD or Regge theory calculations at high energies. As will be shown later, the set of coupling constants and cutoff parameters proposed above are rather well fitted to the relevant experimental data and the results from theoretical calculations with other models.

III. THE $J/\Psi + N \rightarrow \Lambda_c + \bar{D}$ AND $J/\Psi + N \rightarrow \Lambda_c + \bar{D}^*$ REACTIONS

The diagrams for J/Ψ dissociation by a nucleon with the production of the $\Lambda_c + \bar{D}$ and $\Lambda_c + \bar{D}^*$ final states are shown in Figs. 1(a)–1(c). They involve the $J/\Psi \rightarrow D + \bar{D}$ and $J/\Psi \rightarrow D + \bar{D}^*$ vertices and are OZI allowed. These reactions are endothermic, since the total mass of the final states is larger than the total mass of the initial J/Ψ meson and nucleon.

The $J/\Psi + N \rightarrow \Lambda_c + \bar{D}$ reaction via D -meson exchange is shown in the Fig. 1(a) and the corresponding amplitude with an amplitude added in order to preserve gauge invariance in the limit $m_J \rightarrow 0$ may be given by

$$\begin{aligned} \mathcal{M}_a &= 2i g_{JDD} g_{DN\Lambda_c} (\epsilon_J \cdot p_{\bar{D}}) \\ &\times \left(\frac{1}{q^2 - m_D^2} + \frac{1}{2p_J \cdot p_{\bar{D}}} \right) \bar{u}_{\Lambda_c}(p_{\Lambda_c}) \gamma_5 u_N(p_N), \quad (6) \end{aligned}$$

where $q = p_J - p_{\bar{D}} (= p_{\Lambda_c} - p_N)$, while the amplitude via the D^* -meson exchange is shown in Fig. 1(b) and can be written as

$$\begin{aligned} \mathcal{M}_b &= \frac{g_{JD^*D} g_{D^*N\Lambda_c}}{m_J} \frac{1}{q^2 - m_{D^*}^2} \\ &\times \epsilon_{\alpha\beta\mu\nu} p_J^\alpha \epsilon_J^\beta q^\mu \bar{u}_{\Lambda_c}(p_{\Lambda_c}) \gamma^\nu u_N(p_N). \quad (7) \end{aligned}$$

Furthermore, the amplitude for the $J/\Psi + N \rightarrow \Lambda_c + \bar{D}^*$ reaction due to D -meson exchange is shown in Fig. 1(c), and is given by

$$\begin{aligned} \mathcal{M}_c &= \frac{i g_{JDD} g_{DN\Lambda_c}}{m_J} \frac{1}{q^2 - m_D^2} \\ &\times \epsilon_{\alpha\beta\mu\nu} p_J^\alpha \epsilon_J^\beta p_{\bar{D}^*}^\mu \epsilon_{D^*}^\nu \bar{u}_{\Lambda_c}(p_{\Lambda_c}) \gamma_5 u_N(p_N). \quad (8) \end{aligned}$$

In Eqs. (6)–(8) ϵ_J and $\epsilon_{\bar{D}^*}$ are, respectively, the polarization vector of the J/Ψ meson and \bar{D}^* meson, and $q = p_{\Lambda_c} - p_N$ denotes the four-momentum transfer. We notice that there arises no interference term among the amplitudes \mathcal{M}_a , \mathcal{M}_b , and \mathcal{M}_c , because of the Dirac structure, when spin components are not specified and summed over all spins for the N and Λ_c and the different final states.

In our normalization, the corresponding differential cross sections in the center of mass frame of the J/Ψ meson and nucleon system are given by

$$\frac{d\sigma}{d\Omega_{a,b}} = \frac{1}{64\pi^2 s} |\overline{\mathcal{M}_{a,b}}|^2 \times \left(\frac{[(m_{\Lambda_c} + m_D)^2 - s][(m_{\Lambda_c} - m_D)^2 - s]}{[(m_N + m_J)^2 - s][(m_N - m_J)^2 - s]} \right)^{1/2}, \quad (9)$$

$$\frac{d\sigma}{d\Omega_c} = \frac{1}{64\pi^2 s} |\overline{\mathcal{M}_c}|^2 \times \left(\frac{[(m_{\Lambda_c} + m_{D^*})^2 - s][(m_{\Lambda_c} - m_{D^*})^2 - s]}{[(m_N + m_J)^2 - s][(m_N - m_J)^2 - s]} \right)^{1/2}, \quad (10)$$

where $s = (p_N + p_J)^2$ is the squared invariant collision energy and $|\overline{\mathcal{M}_{a,b,c}}|^2$ are the corresponding amplitudes squared, averaged over the initial and summed over the final spins. Explicitly, they are given by

$$|\overline{\mathcal{M}_a}|^2 = \frac{8g_{JDD}^2 g_{D\Lambda_c}^2}{3m_J^2} \left(\frac{1}{q^2 - m_D^2} + \frac{1}{2p_J \cdot p_{\bar{D}}} \right)^2 \times (p_N \cdot p_{\Lambda_c} - m_N m_{\Lambda_c}) [(p_J \cdot p_{\bar{D}})^2 - m_J^2 m_D^2], \quad (11)$$

$$|\overline{\mathcal{M}_b}|^2 = \frac{g_{JD^*D}^2 g_{D^*\Lambda_c}^2}{3m_J^2} \frac{1}{(q^2 - m_{D^*}^2)^2} \times \{ m_J^2 [p^2 q^2 - (m_{\Lambda_c}^2 - m_N^2)^2] + 2(p_J \cdot p)(p_J \cdot q) \times (m_{\Lambda_c}^2 - m_N^2) - p^2 (p_J \cdot q)^2 - q^2 (p_J \cdot p)^2 - 4(p_N \cdot p_{\Lambda_c} - m_N m_{\Lambda_c}) [m_J^2 q^2 - (p_J \cdot q)^2] \}, \quad (12)$$

$$|\overline{\mathcal{M}_c}|^2 = \frac{4g_{JD^*D}^2 g_{D^*\Lambda_c}^2}{3m_J^2} \frac{1}{(q^2 - m_{D^*}^2)^2} (p_N \cdot p_{\Lambda_c} - m_N m_{\Lambda_c}) \times [(p_J \cdot p_{\bar{D}^*})^2 - m_J^2 m_{D^*}^2], \quad (13)$$

with $p \equiv p_{\Lambda_c} + p_N$.

Finally, Fig. 2(a) shows the $J/\Psi + N \rightarrow \Lambda_c + \bar{D}$ cross section as a function of the invariant collision energy \sqrt{s} calculated with D - (solid line) and D^* -meson (dashed line) exchange and with form factors at the interaction vertices. The

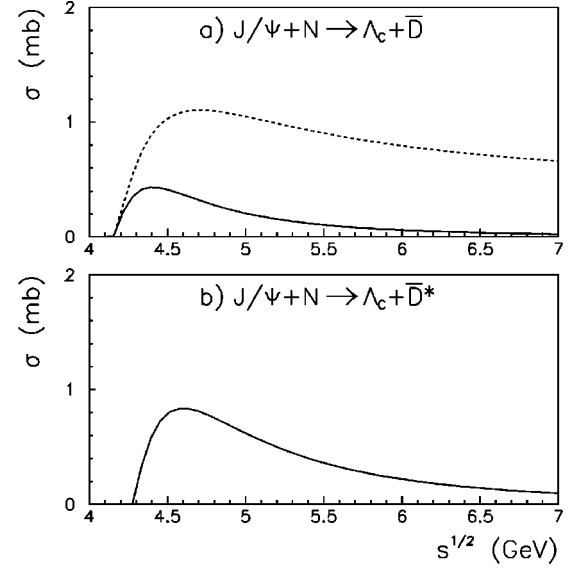


FIG. 2. The cross section for J/Ψ dissociation by the nucleon with $\Lambda_c + \bar{D}$ (a) and $\Lambda_c + \bar{D}^*$ (b) production, as a function of invariant collision energy, \sqrt{s} . The dashed line in (a) shows the calculations involving D^* -meson exchange, while the solid line in (a) indicates the contribution from the D exchange. The results are shown for calculations with form factors introduced at the interaction vertices.

$J/\Psi + N \rightarrow \Lambda_c + \bar{D}^*$ cross section is shown in Fig. 2(b). Both reactions substantially contribute at low energies, close to the respective thresholds, while their contribution to the $J/\Psi + N$ dissociation cross section decreases with increasing \sqrt{s} .

IV. THE $J/\Psi + N \rightarrow N + D + \bar{D}$ REACTION

The diagram for J/Ψ dissociation by a nucleon with the production of the $D + \bar{D}$ state is shown in Fig. 1(d). The dissociation involves the $J/\Psi \rightarrow D + \bar{D}$ vertex and therefore it is an OZI allowed process. The total mass of the produced particles is larger than the total mass of the initial J/Ψ meson and nucleon and thus these reactions are endothermic. Furthermore, the processes with $D + N$ and $\bar{D} + N$ scattering are different and both contribute to J/Ψ dissociation on the nucleon.

The amplitude for the reaction $J/\Psi + N \rightarrow N + D + \bar{D}$ can be parametrized as [22,34]

$$\mathcal{M}_d = 2g_{JDD} \frac{(\epsilon_J \cdot p_D)}{t - m_D^2} F(t) \mathcal{M}_{DN}, \quad (14)$$

where p_D and m_D are the D -meson four-momentum and mass, respectively, ϵ_J denotes the polarization vector of J/Ψ meson, t is squared four-momentum transferred from initial J/Ψ to final D meson, while g_{JDD} and $F(t)$ are the coupling constant and the form factor at the $J/\Psi D \bar{D}$ vertex, respectively. Furthermore, \mathcal{M}_{DN} is the amplitude for $D + N$ or $\bar{D} + N$ scattering, which is related to the physical cross section as

$$|\mathcal{M}_{DN}|^2 = 16\pi s_1 \sigma_{DN}(s_1), \quad (15)$$

where s_1 is the squared-invariant mass of the $D+N$ or $\bar{D}+N$ subsystem.

The double differential cross section for the reaction $J/\Psi + N \rightarrow N + D + \bar{D}$ can be written as

$$\begin{aligned} \frac{d^2\sigma_{JN}}{dt ds_1} &= \frac{g_{JDD}^2}{96\pi^2 q_J^2 s} q_D \sqrt{s_1} \frac{F^2(t)}{(t-m_D)^2} \\ &\times \frac{[(m_J+m_D)^2-t][(m_J-m_D)^2-t]}{m_J^2} \sigma_{DN}(s_1), \end{aligned} \quad (16)$$

where q_D is given by

$$q_D^2 = \frac{[(m_N+m_D)^2-s_1][(m_N-m_D)^2-s_1]}{4s_1}, \quad (17)$$

and m_J and m_N denote the J/Ψ meson and nucleon masses, respectively.

As was proposed in Ref. [34], by replacing the elastic scattering cross section σ_{DN} in Eq. (16) with the total cross section, it is possible to account simultaneously for all available final states that can be produced at the relevant vertex. Since we are interested in inclusive J/Ψ dissociation on the nucleon, in the following we use the total $D+N$ and $\bar{D}+N$ interaction cross sections. However, we denote this inclusive dissociation generically as the $J/\Psi + N \rightarrow N + D + \bar{D}$ reaction.

The total $D+N$ and $\bar{D}+N$ cross sections were evaluated in our previous study [35] by considering the quark diagrammatic approach. It was proposed that the $D+N$ and $\bar{D}+N$ cross sections should be equal to the $\bar{K}+N$ and $K+N$ cross sections, respectively, at the same invariant collision energy and neglecting the contribution from the baryonic resonances coupled to the $\bar{K}+N$ system. The total $\bar{D}+N$ cross section was taken as a constant, $\sigma_{\bar{D}N} = 20$ mb, while the total $D+N$ cross section can be parametrized as

$$\begin{aligned} \sigma_{DN}(s_1) &= \left(\frac{[(m_{\Lambda_c} + m_\pi)^2 - s_1][(m_{\Lambda_c} - m_\pi) - s_1]}{[(m_D + m_N)^2 - s_1][(m_D - m_N) - s_1]} \right)^{1/2} \\ &\times \frac{27}{s_1} + 20, \end{aligned} \quad (18)$$

where m_L and m_π are the Λ_c -hyperon and pion masses, respectively, given in GeV and the cross section is given in millibarn.

Some of the partial $D+N$ cross sections were calculated in Ref. [21] by an effective Lagrangian approach, where the identity between the $\bar{K}+N$ and $D+N$ interaction was imposed by the SU(4) relations. Indeed, on the basis of SU(4) symmetry the couplings for the vertices containing \bar{K} or K mesons were taken to be equal to those obtained by replacing \bar{K} or K with D or \bar{D} , respectively. For instance, $g_{\pi DD^*}$

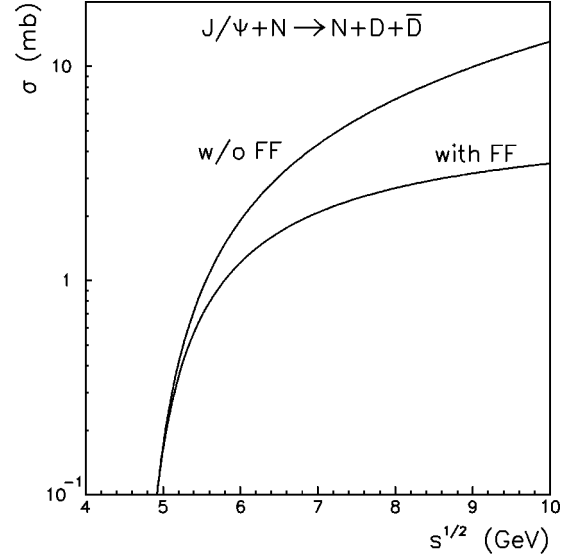


FIG. 3. The cross section for J/Ψ dissociation by the nucleon with $\bar{D}+D$ production as a function of invariant collision energy \sqrt{s} . The results are shown for calculations with and without form factor at the $J/\Psi\bar{D}D$ vertex.

$= g_{\pi KK^*}$, $g_{DN\Lambda_c} = g_{KNA}$, etc. In the more general case, the large variety of possible diagrams describing the $\bar{K}+N$ and $K+N$ interactions can be identified to those for the $D+N$ and $\bar{D}+N$ interactions, respectively. Thus, the estimates given in Ref. [35] are supported by the boson-exchange formalism. The comparison between the DN scattering cross section calculated by an effective Lagrangian and evaluated by the quark diagrammatic approaches is given in Ref. [36]. Furthermore, for the $J/\Psi + N \rightarrow N + D + \bar{D}$ calculations we used coupling constants and form factors similar to those used for the $J/\Psi + N \rightarrow \Lambda_c + \bar{D}$ reaction.

Figure 3 shows the cross section for J/Ψ dissociation on the nucleon with the production of $\bar{D}+D$ pairs calculated using Eq. (16), with and without a form factor at the $J/\Psi\bar{D}D$ vertex. The lines in Fig. 3 show the results, where the processes with $\bar{D}+N$ and $D+N$ interactions were summed incoherently.

V. TOTAL $J/\Psi + N$ CROSS SECTION AND COMPARISON WITH QCD CALCULATIONS

Our results for the total $J/\Psi + N$ cross section are shown in Fig. 4 as the solid line (a). Here the total cross section is given as a sum of the partial $J/\Psi + N \rightarrow \Lambda_c + \bar{D}$ cross section calculated with D^- and D^* -meson exchange, the $J/\Psi + N \rightarrow \Lambda_c + \bar{D}^*$ cross section calculated with D -meson exchange and the inclusive cross section for J/Ψ dissociation with $\bar{D}+D$ production.

We found that the total $J/\Psi + N$ cross section approaches 5.5 mb at high invariant collision energy. We also indicate a partial enhancement of the $J/\Psi + N$ dissociation cross section at low energies due to the contribution from the J/Ψ

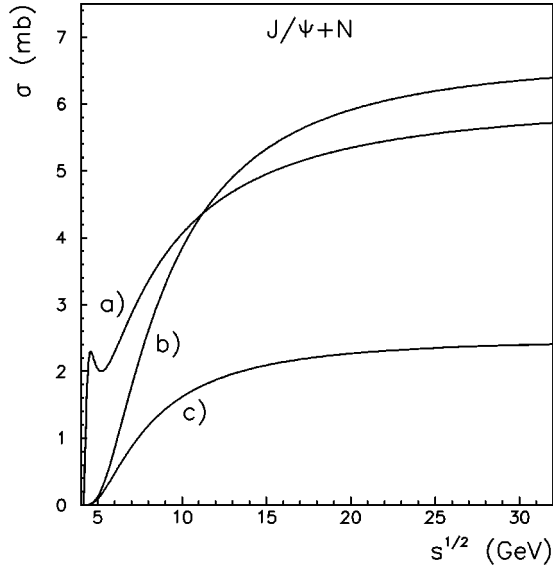


FIG. 4. The total cross section for J/Ψ dissociation by the nucleon as a function of invariant collision energy \sqrt{s} . Line (a) shows our calculation with form factors. Line (b) indicates the first order calculations based on a short distance QCD, while line (c) shows the parametrization from Ref. [37].

$+N \rightarrow \Lambda_c + \bar{D}$ and $J/\Psi + N \rightarrow \Lambda_c + \bar{D}^*$ reaction channels.

The line (c) in Fig. 4 shows the parametrization from Ref. [37], explicitly given as

$$\sigma_{JN} = 2.5 \left(1 - \frac{\lambda}{\lambda_0} \right)^{6.5}, \quad (19)$$

where the cross section is given in millibar, $\lambda_0 = m_N + \epsilon_0$ with ϵ_0 being the Rydberg energy and

$$\lambda = \frac{s - m_J^2 - m_N^2}{2m_J}. \quad (20)$$

Parametrization (20) provides a substantially smaller J/Ψ dissociation cross section compared to our result.

Furthermore, the $J/\Psi + N$ cross section can be evaluated [38,39] using short-distance QCD methods based on the operator-product expansion [40]. Within the first order calculation, the cross section is given as [41]

$$\sigma_{JN} = \frac{2^{13} \pi}{3^4 \alpha_s m_c^2} \int_{1/\xi}^1 \frac{(\xi x - 1)^{3/2} g(x)}{(\xi x)^5 x} dx, \quad (21)$$

where $\xi = \lambda/\epsilon_0$, m_c is the c quark mass, α_s is the strong coupling constant, and $g(x)$ denotes the gluon distribution function, for which we take the form

$$g(x) = 2.5(1-x)^4. \quad (22)$$

Calculations with a more realistic gluon distribution function [42] only change the $J/\Psi + N$ cross section slightly at invariant collision energies $\sqrt{s} < 20$ GeV, as compared to that obtained with function (22). The differences associated with various gluon structure functions can be predominantly ob-

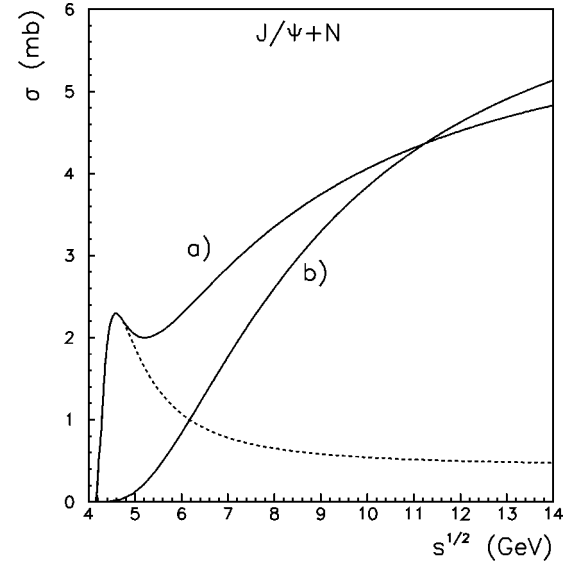


FIG. 5. The total cross section for J/Ψ dissociation by the nucleon as a function of invariant collision energy \sqrt{s} . Solid line (a) shows our calculations with form factors, while the dashed line indicates the contribution from the $J/\Psi + N \rightarrow \Lambda_c + \bar{D}$ and $J/\Psi + N \rightarrow \Lambda_c + \bar{D}^*$ reaction channels only. Solid line (b) indicates the first order calculation based on short-distance QCD.

served at high \sqrt{s} . The $J/\Psi + N$ cross section from the first order calculations performed using short-distance QCD is shown by line (b) in Fig. 4.

We note that the QCD results are in good agreement with our hadronic model calculations at high invariant collision energies, but substantially deviate from our predictions near the threshold for endothermic reaction. We ascribe this discrepancy to the contribution from the $J/\Psi + N \rightarrow \Lambda_c + \bar{D}$ and $J/\Psi + N \rightarrow \Lambda_c + \bar{D}^*$ reactions. The dashed line in Fig. 5 shows separate contribution to the total $J/\Psi + N$ cross section from the $J/\Psi + N \rightarrow \Lambda_c + \bar{D}$ and $J/\Psi + N \rightarrow \Lambda_c + \bar{D}^*$ reactions, while solid line (a) again shows our result for the total J/Ψ dissociation by a nucleon. Solid line (b) in Fig. 5 indicates the QCD result given by Eq. (21). It is clear that the main difference between our prediction and the QCD calculation comes from the $J/\Psi + N \rightarrow \Lambda_c + \bar{D}$ and $J/\Psi + N \rightarrow \Lambda_c + \bar{D}^*$ reaction channels, which contributes substantially at low \sqrt{s} .

VI. J/Ψ PHOTOPRODUCTION ON THE NUCLEON

Within the vector-dominance model, the J/Ψ photoproduction invariant amplitude $\mathcal{M}_{\gamma J}$ on a nucleon can be related to the $J/\Psi + N$ scattering amplitude \mathcal{M}_{JN} as

$$\mathcal{M}_{\gamma J}(s, t) = \frac{\sqrt{\pi} \alpha}{\gamma_J} F(t) \mathcal{M}_{JN}(s, t), \quad (23)$$

where s is the squared invariant collision energy, t is the squared four-momentum transfer, α is the fine-structure constant, and γ_J is the constant for J/Ψ coupling to the photon. In Eq. (23) $F(t)$ stands for the form factor at the $\gamma - J/\Psi$

vertex, which accounts for the $c\bar{c}$ fluctuation of the photon [43]. Within the naive VDM, only the hadronic but not the quark-antiquark fluctuations of the photon through the γ mixing with the vector mesons are considered [44,45] and the form factor $F(t)$ in Eq. (23) is therefore neglected. As was calculated in Ref. [43] by both the hadronic and quark representations of the $c\bar{c}$ fluctuation of the photon, the form factor $F=0.3$ at $t=0$.

The invariant amplitudes are normalized so that the $J/\Psi + N$ differential cross section is written as

$$\frac{d\sigma}{dt} = \frac{|\mathcal{M}|^2}{16\pi[(s-m_N^2-m_J^2)^2-4m_N^2m_J^2]}, \quad (24)$$

and similarly for the J/Ψ photoproduction cross section.

Taking the relation of Eq. (23) at $t=0$ and applying the optical theorem for the imaginary part of the $J/\Psi + N$ scattering amplitude, one can express the total cross section for J/Ψ dissociation by a nucleon σ_{JN} in terms of the cross section for J/Ψ photoproduction on the nucleon at $t=0$ as

$$\left. \frac{d\sigma_{\gamma N \rightarrow JN}}{dt} \right|_{t=0} = \frac{\alpha}{16\gamma_J^2} (1 + \alpha_{JN}^2) \sigma_{JN}^2 F^2(0) \times \frac{(s-m_N^2-m_J^2)^2-4m_N^2m_J^2}{(s-m_N^2)^2}, \quad (25)$$

where α_{JN} is the ratio of the real to imaginary part of the $J/\Psi + N$ scattering amplitude at $t=0$.

The γ_J coupling constant can be directly determined from the J/Ψ meson decay into leptons [46]

$$\Gamma(J/\Psi \rightarrow l^+ l^-) = \frac{\pi\alpha^2}{3\gamma_J^2} \sqrt{m_J^2-4m_l^2} \left[1 + \frac{2m_l^2}{m_J^2} \right]. \quad (26)$$

The ratio α_{JN} is unknown and as a first approximation we put it equal to zero. This approximation is supported from two sides.

At high energies, Regge theory dictates that the amplitude for hadron scattering on a nucleon is dominated by pomeron exchange and is therefore purely imaginary. This expectation is strongly supported by the experimental data [47] available for p , $\bar{p}\pi$, K , and \bar{K} scattering by a nucleon.

At low energies, the real part of the $J/\Psi + N$ scattering amplitude at $t=0$ can be estimated from the theoretical calculations of the J/Ψ meson mass shift in nuclear matter. As was predicted by the calculations by the operator-product expansion [48,49], QCD van der Waals potential [50], and QCD sum rules [51–53], the mass of the J/Ψ should only be charged by a tiny amount in nuclear matter. However, a partial deviation of our results from the J/Ψ photoproduction data might be actually addressed to the contribution from a nonvanishing ratio α_{JN} . More detailed discussion concerning an evaluation of the real part of the $J/\Psi + N$ scattering amplitude will be given in the following.

The J/Ψ photoproduction cross section at $t=0$ is shown in Fig. 6 as a function of the invariant collision energy. The experimental data were taken from Refs. [54–56]. The solid

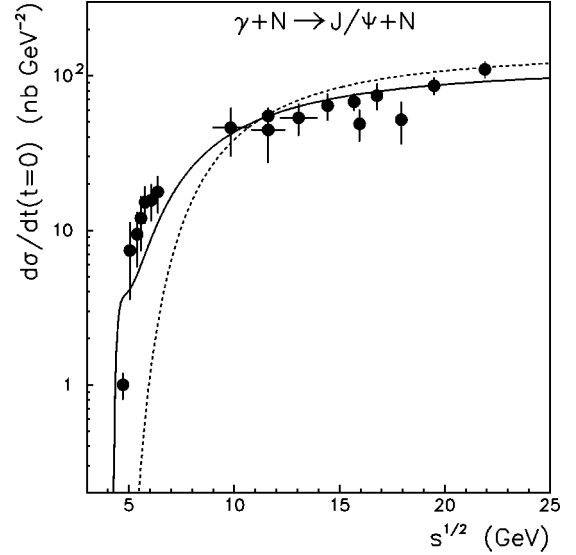


FIG. 6. Differential cross section for the reaction $\gamma + N \rightarrow J/\Psi + N$ at $t=0$ as a function of the invariant collision energy \sqrt{s} . Experimental data are from Refs. [54–56]. The solid line shows our calculations with the total $J/\Psi + N$ dissociation cross section evaluated using a boson-exchange model, while the dashed line indicates the results obtained for the $J/\Psi + N$ cross section given by short-distance QCD.

line shows the results calculated with the total $J/\Psi + N$ cross section given by the boson-exchange model. We found that within the experimental uncertainties we can reproduce the J/Ψ photoproduction data at $t=0$ at low energies quite well. Let us recall that this is possible because of the contribution from the $J/\Psi + N \rightarrow \Lambda_c + \bar{D}$ and $J/\Psi + N \rightarrow \Lambda_c + \bar{D}^*$ reaction channels.

The dashed line in Fig. 6 indicates the calculations using Eq. (21), which reasonably describe the data on photoproduction cross section at $\sqrt{s} > 10$ GeV. We notice a reasonable agreement between our calculations and the results from short-distance QCD at invariant collision energies $\sqrt{s} > 12$ GeV. We also recall that in Ref. [39] the discrepancy between the QCD results and the photoproduction data at low \sqrt{s} was attributed to a large ratio α_{JN} . Our result does not support this suggestion.

VII. COMPARISON WITH REGGE THEORY

It is of some interest to compare our results with the predictions from Regge theory [57] given at high energies. Furthermore, for illustrative purpose we demonstrate the comparison in terms of the cross section at $t=0$ for the $\gamma + N \rightarrow J/\Psi + N$ reaction, since the Regge model parameters were originally fitted to the photoproduction data.

Taking into account the contribution from soft- and hard-pomeron exchanges alone, the exclusive J/Ψ photoproduction cross section at $t=0$ can be explicitly written as [58]

$$\left. \frac{d\sigma}{dt} \right|_{t=0} = 23.15s^{0.16} + 0.034s^{0.88} + 1.49s^{0.52}, \quad (27)$$

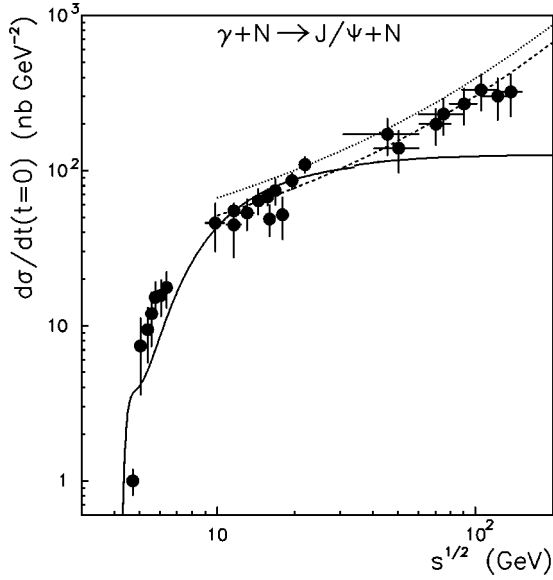


FIG. 7. The cross section for the reaction $\gamma+N \rightarrow J/\Psi+N$ at $t=0$ as a function of invariant collision energy \sqrt{s} . Experimental data are from Refs. [54–56,63,64]. The solid line shows our calculations with the total $J/\Psi+N$ dissociation cross section evaluated by boson-exchange model. The dotted line shows the prediction (27) from Regge theory with parameters for the soft and hard pomeron from Ref. [59], while the dashed line is the result given by Eq. (27), but renormalized by the factor 1.3.

where the cross section is given in nanobarn and the squared invariant collision energy s is in GeV^2 . The first term of Eq. (27) comes from the soft pomeron contribution, the second one is due to the hard pomeron, while the last term stems from their interference. The parameters for the both pomeron trajectories were taken from the most recent fit [59] to the J/Ψ photoproduction data from H1 [60] and ZEUS [61,62] experiments.

The prediction from Regge theory is shown by the dotted line in Fig. 7 together with experimental data [54–56,63,64] on J/Ψ photoproduction cross section at $t=0$ as a function of the invariant collision energy \sqrt{s} . The solid line in Fig. 7 shows our calculations using the boson-exchange model with form factors. We notice, that in Refs. [57,59] the Regge model fit to the data on $\gamma+N \rightarrow J/\Psi+N$ cross section at $t=0$ was not explicitly included in an evaluation of the coefficients of Eq. (27), which might partially explain some systematic deviation of the Regge calculations from the photoproduction data.

In order to illustrate the compatibility of the Regge model prediction with our calculations we indicate by the dashed line in Fig. 7 the result from Eq. (27), renormalized by a factor 1.3. We note a reasonable agreement between our calculations and the Regge theory within the short range of energies from $\sqrt{s} \approx 10$ to 30 GeV.

However, considering the results given in this section, one should keep in mind the following critical arguments.

First, we performed the calculations using a boson-exchange model, which has some restrictions in its application at high energies. For instance, the form factors introduced at the interaction vertices suppress the contribution at

large four-momentum transfer t , which allows one to avoid the divergence of the total cross section at large collision energies where the range of the available t becomes extremely large [22]. A more accurate way to resolve such a divergence at high energies is to use the Reggeized boson-exchange model [65–67].

Second, the Regge theory has limitations for applications at low energies [47]. Here we adopt the parameters for soft- and hard-pomeron trajectories that were originally fixed [59] using the large set of data at $\sqrt{s} \geq 40$ GeV and the very reasonable agreement between the Regge model calculations with the data, even at lower energies, might in some sense be viewed as surprising.

On the other hand, the D - and D^* -meson exchanges used in our calculations cannot be related to pomeron exchange, rather they can be related to the Regge trajectories, whose contribution to J/Ψ photoproduction at high energies was assumed [57–59] to be negligible. This does not contradict the results shown in Fig. 7, since our calculations are substantially below the data at high energies.

VIII. EVALUATION OF THE REAL PART OF $J/\Psi+N$ SCATTERING AMPLITUDE

One of the crucial ways to test the coherence of our calculations consists of an evaluation of the real part of the $J/\Psi+N$ scattering amplitude at $t=0$ and a comparison to the various model predictions [51–53] for $\text{Re} f(0)$ at zero J/Ψ momentum. The latter is of course related to the J/Ψ meson mass shift or the real part of its potential in nuclear matter.

Within the low density theorem the J/Ψ meson mass shift Δm_J in nuclear matter at baryon density ρ_B can be related to the real part of the scattering amplitude $\text{Re} f(0)$ as [52,68,69]

$$\Delta m_J = -2\pi \frac{m_N + m_J}{m_N m_J} \rho_B \text{Re} f(0). \quad (28)$$

The recent QCD sum rule analysis [51–53] with the operator-product expansion predicts attractive mass shifts of about -4 to -10 MeV for J/Ψ meson in nuclear matter, which corresponds to small $\text{Re} f(0)$ about 0.1 to 0.2 fm. This result is very close to the predictions from the operator-product expansion [48,49] and the calculations with QCD van der Waals potential [50].

There are two ways to link these results for the effective J/Ψ mass in nuclear matter or the J/Ψ nucleon scattering length with our calculations. Both the methods applied below contain a number of uncertainties and should be carefully considered.

First, we address the partial discrepancy between our calculations of the J/Ψ photoproduction cross section at $t=0$ and data at low energies due to the nonzero ratio α_{JN} appearing in Eq. (25) and evaluate it from the experimental measurements as

$$\alpha_{JN}^2 = \frac{d\sigma^{\text{exp}}}{dt} \Big|_{t=0} \left[\frac{d\sigma^{\text{th}}}{dt} \Big|_{t=0} \right]^{-1} - 1, \quad (29)$$

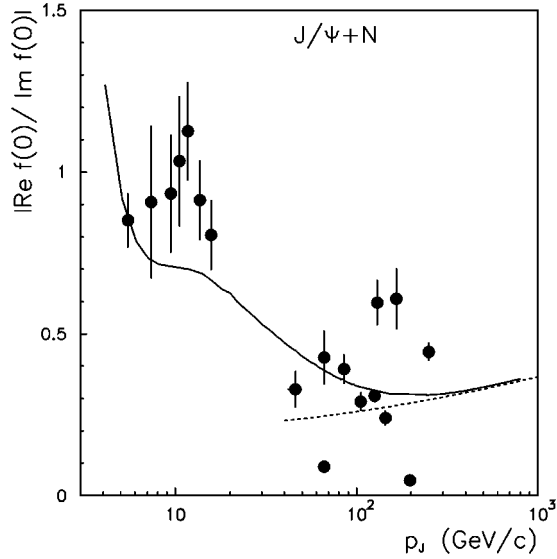


FIG. 8. The modulus of the ratio of real to imaginary part of the $J/\Psi + N$ scattering amplitude at $t=0$ extracted from experimental data on cross section for $\gamma + N \rightarrow J/\Psi + N$ reaction as a function of J/Ψ momentum p_J in the nucleon rest frame. Experimental data used in the evaluation are from Refs. [54–56]. The solid line shows the results from the dispersion relation. The dotted line shows the prediction from Regge theory, which fixed the positive sign of the ratio.

where the indices exp and th denote the experimental and theoretical results for the photoproduction cross section at $t=0$, respectively.

The modulus of the ratio α_{JN} evaluated from the data is shown in Fig. 8 as a function of the J/Ψ momentum p_J in the nucleon rest frame. It is clear that the sign of the ratio cannot be fixed by Eq. (29), but some insight might be gained from the Regge theory calculation, which is shown in Fig. 8 by the dashed line. Here again we use the parameters of the pomeron trajectories from Ref. [59]. Now one can conclude that the $\text{Re} f(0)$ is positive at low J/Ψ momenta, which agrees with the predictions [48–53] on the reduction of the J/Ψ meson mass in nuclear matter. However, this speculation is true only if the real part of the J/Ψ nucleon scattering amplitude at $t=0$ does not change its sign at some moderate momentum.

Now, $\text{Re} f(0)$ is given as a product of the ratio α_{JN} extracted from the photoproduction data [54–56] and the imaginary part of the $J/\Psi + N$ scattering amplitude at $t=0$, which is related to the total $J/\Psi + N$ cross section by the optical theorem (30) as

$$\text{Im} f(0) = \frac{p_J}{4\pi} \sigma_{JN}. \quad (30)$$

Let us recall that in our calculations the total $J/\Psi + N$ cross section is given only for OZI allowed processes, i.e., at energies $\sqrt{s} \geq m_{\Lambda_c} + m_D$. This threshold corresponds to the J/Ψ meson momentum of ≈ 1.88 GeV/c. Thus, within the present method we cannot provide the real part of the scattering amplitude at $p_J=0$ and make a direct comparison with

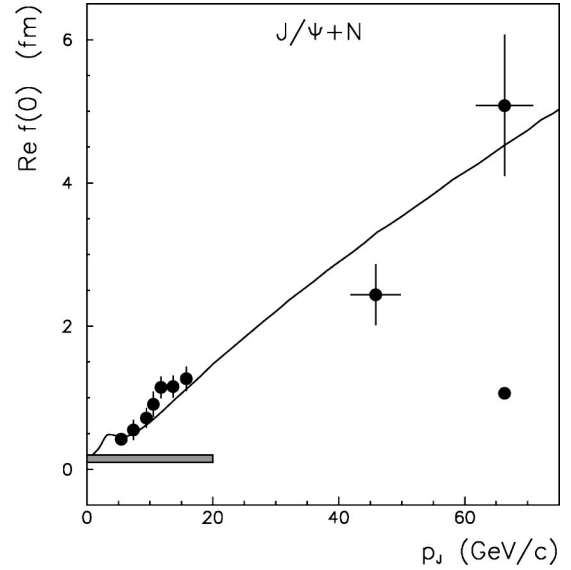


FIG. 9. The real part $\text{Re} f(0)$ of the $J/\Psi + N$ scattering amplitude extracted from experimental data [54–56] on the cross section for $\gamma + N \rightarrow J/\Psi + N$ reaction at $t=0$ as a function of J/Ψ momentum p_J in the nucleon rest frame. The solid line shows the $\text{Re} f(0)$ evaluated using the dispersion relation. The shadowed area indicates the range of the predictions from Refs. [48–53] given at zero momentum of the J/Ψ meson. The extension of the shadowed area to higher momenta is shown only for orientation and has no physical meaning.

the absolute value of the $\text{Re} f(0)$ predicted in Refs. [48–53]. However, the estimate of $\text{Re} f(0)$ at minimal J/Ψ momenta allowed by OZI reactions might be done.

The $\text{Re} f(0)$ extracted from the experimental data on J/Ψ meson photoproduction cross section on a nucleon at $t=0$ is shown in Fig. 9 as a function of J/Ψ momentum in the nucleon rest frame. The shadowed area shows the predictions [48–53] at $p_J=0$. Notice, that the shadowed area is extended to higher momenta only for orientation. Within the uncertainties of the method we could not detect any discrepancy with the absolute value of the $\text{Re} f(0)$ given in Refs. [48–53]. However, we emphasize again, that this conclusion should be accepted very carefully.

A different way to evaluate the real part of the $J/\Psi + N$ scattering amplitude at $t=0$ involves the dispersion relation that is given as [70]

$$\text{Re} f(\omega) = \text{Re} f(\omega_0) + \frac{2(\omega^2 - \omega_0^2)}{\pi} \times P \int_{\omega_{\min}}^{\infty} \frac{\omega' \text{Im} f(\omega')}{(\omega'^2 - \omega_0^2)(\omega'^2 - \omega^2)} d\omega', \quad (31)$$

where ω stands for the J/Ψ total energy, ω_{\min} is the threshold energy, and $\text{Im} f(\omega)$ denotes the imaginary part of the J/Ψ nucleon scattering amplitude at $t=0$, as a function of energy ω , which can be evaluated from Eq. (30). Furthermore, $\text{Re} f(\omega_0)$ is the subtraction constant taken at J/Ψ energy ω_0 .

Being more fundamental, this method involves substantial uncertainties for the following reasons. First, we should specify the subtraction constant. By taking it at $p_J=0$ from Eq. (28) we could not further verify the consistency of our calculations with the predictions from Refs. [48–53]. Second, to evaluate the principal value of the integral of Eq. (31) one should know the imaginary part of the $J/\Psi + N$ scattering amplitude at $t=0$ or the total cross section up to infinite energy.

Since our model could not provide the high energy behavior of σ_{JN} one should make an extrapolation to high energies by using either short-distance QCD or Regge theory. As was shown in Ref. [39] the total $J/\Psi + N$ cross section at high energies is dependent on the gluon distribution function $g(x)$ appearing in Eq. (21). Furthermore, both distributions given by Eq. (22) and taken from Ref. [42] were unable to reproduce [39] the experimental data on the $\gamma + N \rightarrow J/\Psi + N$ cross section at $\sqrt{s} > 70$ GeV. Thus we could not extrapolate our results to high energies by the short-distance QCD calculations.

As shown in Fig. 7, the Regge theory reproduces the J/Ψ photoproduction data at $t=0$ quite well when renormalized by a factor of 1.3. This meets our criteria since it also fits our calculations at $\sqrt{s} \approx 20$ GeV. Thus we adopt the Regge-model fit for the extrapolation of our results to high energies in order to evaluate the dispersion relation. It is important to notice, that, in principle, there is no need to address J/Ψ photoproduction in order to extrapolate our results to infinite energy using Regge theory. One can adopt the energy dependence of the dissociation cross section given by soft- and hard-pomeron exchanges and make the absolute normalization by our calculations $\sqrt{s} > 20$ GeV. This is reasonable, because the absolute normalization from the Regge model can be considered to some extent as a free parameter, not fixed by the theory.

Moreover, we take the subtraction constant $\text{Re}f(\omega_0)$ at high energy, $\omega_0 = 10^3$ GeV, and fix it by Regge theory with the predicted ratio α_{JN} . Thus we can independently use an evaluated real part of the $J/\Psi + N$ scattering amplitude at $t=0$ for comparison with the predictions [48–53] given at $p_J=0$.

Our results for the ratio α_{JN} evaluated by the dispersion relation (31) are shown in Fig. 8 by the solid line. Obviously, the calculations match the Regge model predictions since they were used to fix both the high energy behavior of the total $J/\Psi + N$ cross section and the subtraction constant for the real part of the scattering amplitude at $t=0$. Furthermore, the dispersion calculations give a surprisingly good fit to the ratios α_{JN} extracted from the experimental data [54–56] on the cross section at $t=0$ of the $\gamma + N \rightarrow J/\Psi + N$ reaction.

The real part of the $J/\Psi + N$ scattering amplitude calculated by dispersion relation is shown by the solid line in Fig. 9 as a function of J/Ψ meson momentum in the nucleon rest frame. Our calculations describes reasonably well the data evaluated from the J/Ψ photoproduction at $t=0$, that are shown by the solid circles in Fig. 9. It is important that our results, normalized by a subtraction constant at high energies $p_J = 10^3$ GeV, simultaneously match the predictions [48–53] given at $p_J=0$.

Concluding this section let us make a few remarks. The two methods applied to the evaluation of the real part of the J/Ψ nucleon scattering amplitude at $t=0$ are actually different, but nevertheless provide almost identical results for the $\text{Re}f(0)$ over a large range of J/Ψ momenta. The consistency of our approach can be proved by agreement between our calculations simultaneously with the Regge model predictions for $\text{Re}f(0)$ at high energy and the predictions from various models [48–53] for $\text{Re}f(0)$ at $p_J=0$. From these results we confirm that below the momentum of $p_J \approx 1.88$ GeV, which corresponds to the OZI allowed $J/\Psi + N \rightarrow \Lambda_c + \bar{D}$ threshold, the J/Ψ interactions with a nucleon are purely elastic. The J/Ψ meson does not undergo significant dissociation on absorption at momenta $p_J < 1.88$ GeV.

IX. ESTIMATE OF THE ELASTIC $J/\Psi + N$ CROSS SECTION

By definition, the total elastic $J/\Psi + N \rightarrow J/\Psi + N$ cross section σ_{el} is related to the elastic differential cross section as

$$\sigma_{\text{el}} = \int \left. \frac{d\sigma}{dt} \right|_{t=0} \exp(bt), \quad (32)$$

where b is an exponential slope of the differential cross section and the cross section as the optical point $t=0$ is related to the total $J/\Psi + N$ cross section and the ratio α_{JN} of the real and imaginary part of the scattering amplitude as

$$\left. \frac{d\sigma}{dt} \right|_{t=0} = \frac{1}{16\pi} (1 + \alpha_{JN}^2) \sigma_{JN}^2. \quad (33)$$

The slope b can be estimated from the differential $\gamma + N \rightarrow J/\Psi + N$ cross section and was fitted in Ref. [39] to available experimental data as $b = -1.64 + 0.83 \ln s$.

Finally, the elastic $J/\Psi + N$ cross section is given by

$$\sigma_{\text{el}} = \frac{1}{16\pi b} (1 + \alpha_{JN}^2) \sigma_{JN}^2, \quad (34)$$

and is shown in Fig. 10 as a function of J/Ψ meson momentum. The dashed area in Fig. 10 indicates the elastic cross section at $p_J=0$ given within the scattering length approximation in Refs. [48–53] as

$$\sigma_{\text{el}} = 4\pi |\text{Re}f(0)|^2, \quad (35)$$

that is valid as far as $\text{Im}f(0)=0$ at $p_J=0$. Note, that Eq. (34) could not provide the estimate for elastic cross section at $p_J < 1.88$ GeV, i.e., below the $\Lambda_c + \bar{D}$ reaction threshold, where the dissociation cross section $\sigma_{JN}=0$. In principle, one can interpolate σ_{el} from zero J/Ψ momentum to our results.

As we discussed already, the uncertainty in the elastic cross section at $p_J=0$, given in Refs. [48–53], is very large and to make a less unambiguous interpolation let us use only the most recent results from the QCD sum rule calculations [51–53]. Let us recall that the QCD sum rule calculations

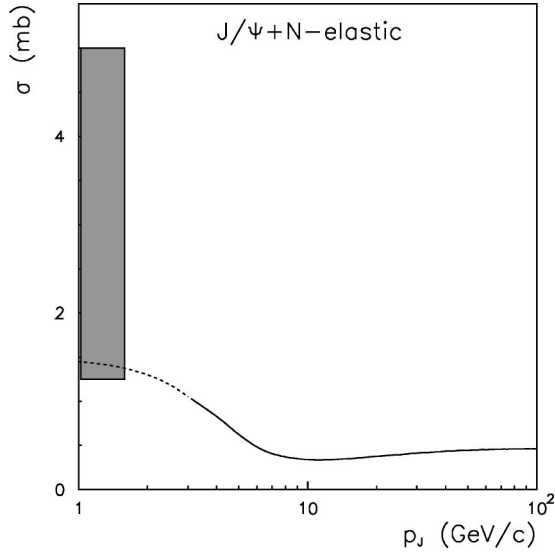


FIG. 10. The elastic $J/\Psi + N$ cross section as a function of the J/Ψ meson momentum in the nucleon rest frame. The solid lines show our calculations. The dashed area illustrates predictions from Refs. [48–53] given at $p_J=0$. The dashed line indicates our interpolation for the elastic cross section based on the QCD sum rule results alone [51–53].

from Ref. [51] indicate a shift of the J/Ψ mass of about -5 to -10 MeV, while in Ref. [52] the mass shift was reported to be in the range $-7 \leq \Delta m_J \leq -4$ MeV. The calculations with higher dimension operators in the QCD sum rule provide [53] $\Delta m_J = -4$ MeV. Thus, we take an average value that corresponds to $\sigma_{\text{el}} = 1.6$ mb at $p_J = 0$. Now the dashed line in Fig. 10 indicates our interpolation of the elastic cross section at low momenta.

Furthermore, the vector dominance model can be used to relate the elastic $J/\Psi + N \rightarrow J/\Psi + N$ cross section σ_{el} and the total $\gamma + N \rightarrow J/\Psi + N$ cross section $\sigma_{\gamma J}$. Applying Eq. (23) and neglecting the form factor this relation can be written as

$$\sigma_{\text{el}} = \frac{\gamma_J^2}{\pi \alpha} \frac{(s - m_J^2)^2}{(s - m_N^2 - m_J^2)^2 - 4m_N^2 m_J^2} \sigma_{\gamma J}. \quad (36)$$

Figure 11(a) shows the $\gamma + N \rightarrow J/\Psi + N$ cross section [71] as a function of invariant collision energy, while the elastic cross section σ_{el} evaluated from experimental photoproduction data using Eq. (36) is shown in Fig. 11(b). Apart from the absolute value of the σ_{el} , which is substantially below our estimate, we notice that very strong energy dependence of the elastic $J/\Psi + N \rightarrow J/\Psi + N$ cross section evaluated using Eq. (36) might alone indicate the inconsistency of the application of naive VDM [43]. Indeed, as we discussed above, the calculations of the J/Ψ mass shift in matter or $J/\Psi + N$ scattering length given in Refs. [48–53] predict the elastic cross section in the range $1.25 \leq \sigma_{\text{el}} \leq 5$ mb at $p_J = 0$, while the J/Ψ meson photoproduction data evaluated by Eq. (36) indicate a systematic decrease of σ_{el} with decrease of J/Ψ meson momentum.

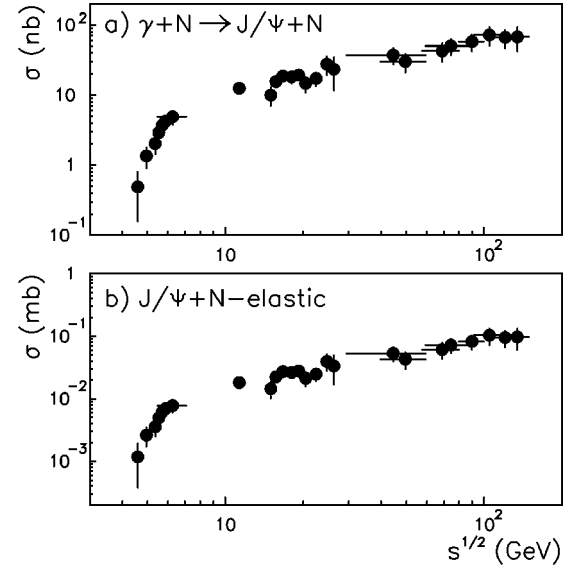


FIG. 11. The total $\gamma + N \rightarrow J/\Psi + N$ cross section (a) collected in Ref. [71] and the elastic $J/\Psi + N \rightarrow J/\Psi + N$ cross section (b) evaluated by naive vector dominance given by Eq. (36) as a function of the invariant collision energy \sqrt{s} .

Apparently this inconsistency might be resolved by introducing a form factor $F(t)$ at the $\gamma - J/\Psi$ vertex [43], as given by Eq. (23) and applied in our study. The correction to the naive vector dominance is then given as

$$\kappa = \left[\int \exp(bt) \right]^{-1} \int F^2(t) \exp(bt), \quad (37)$$

where b is the slope of the differential $\gamma + N \rightarrow J/\Psi + N$ cross section and the integration in Eq. (37) is performed over the range of the squared-transverse momentum t available at given invariant collision energy \sqrt{s} .

By taking, for simplicity, an exponential form of the $\gamma - J/\Psi$ form factor with cutoff parameter $\Lambda = 1.7 \text{ GeV}^{-2}$, we evaluate the elastic $J/\Psi + N \rightarrow J/\Psi + N$ cross section from the data on the $\gamma + N \rightarrow J/\Psi + N$ cross section [71] and show the result by the circles in Fig. 12, as a function of the J/Ψ meson momentum. The solid line in Fig. 12 indicates our estimate for σ_{el} , which clearly give a reasonable fit to the correctly extracted data over a large range of available momenta p_J .

It is worthwhile to note that Fig. 12 clearly illustrates that the introduction of a form factor at the $J/\Psi - N$ vertex allows one to resolve an inconsistency in the evaluation, the elastic $J/\Psi + N \rightarrow J/\Psi + N$ cross section from the total $\gamma + N \rightarrow J/\Psi + N$ cross section.

X. FINAL RESULTS

Finally, Fig. 13 shows the $J/\Psi + N$ dissociation and elastic cross sections over a large range of J/Ψ momenta. Let us recall that the dissociation cross section σ_{JN} was calculated using the boson-exchange model up to $p_J \approx 200 \text{ GeV}/c$ and extrapolated to high energies by Regge theory.

Now we compare our results with the $J/\Psi + N$ dissocia-

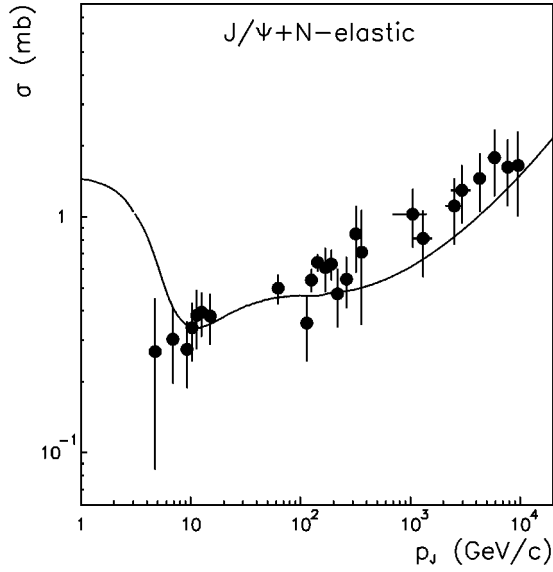


FIG. 12. The circles show the elastic $J/\Psi + N \rightarrow J/\Psi + N$ cross section as a function of the J/Ψ momentum evaluated from the total $\gamma + N \rightarrow J/\Psi + N$ cross section by vector dominance model of Eq. (36) additionally corrected by the factor κ given by Eq. (37). The solid line indicates our estimate for σ_{el} calculated by Eq. (34).

tion cross section evaluated from nuclear reactions. The square in Fig. 13 shows the σ_{JN} extracted from the J/Ψ photoproduction from nuclei at a mean photon energy of 17 GeV [11]. The J/Ψ meson momentum was not explicitly fixed and is indicated in Fig. 13 only for orientation.

Furthermore, the circle indicates the result from the combined analysis [12] of experimental data on J/Ψ production

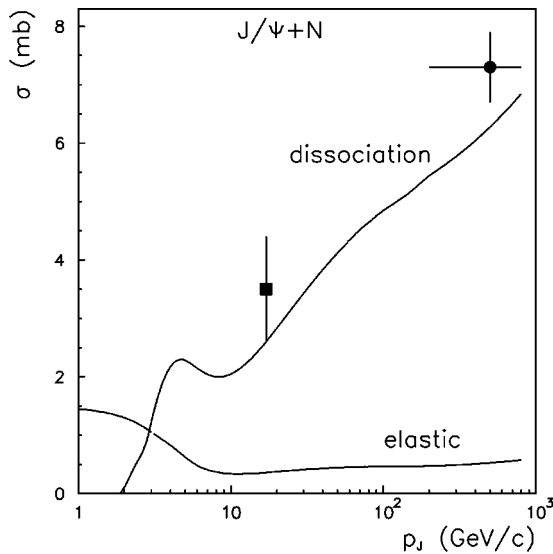


FIG. 13. The elastic and dissociation ($J/\Psi + N$) cross sections as a function of the J/Ψ meson momentum in the nucleon rest frame. The solid lines show our results. The square shows the $J/\Psi + N$ dissociation cross section evaluated from J/Ψ photoproduction on nuclei, while the circle indicates the dissociation cross section evaluated from J/Ψ production from proton-nucleus collisions.

from $p + A$ collisions at beam energies from 200 to 800 GeV. Again the J/Ψ meson momentum was not explicitly fixed by the analysis [12].

Within the experimental uncertainties, our results for the total $J/\Psi + N$ dissociation cross section fit the available experimental data reasonably well.

We notice, that our results slightly ($\approx 15\%$) underestimate the $J/\Psi + N$ dissociation cross section evaluated from experimental data on J/Ψ production from $\gamma + A$ and $p + A$ reactions.

We also note that the NA50 experimental data on J/Ψ production from heavy ion collisions [1] can be reasonably well fitted by the calculations [6,7,72] with a $J/\Psi + N$ dissociation cross section $\sigma_{JN} \approx 3 - 6.7$ mb. The most recent calculations [2-4] on J/Ψ production and comparison to NA50 data [1] indicates a smaller dissociation cross section, in the range from 3 to 4.5 mb. In central Pb+Pb collisions at 160A GeV the J/Ψ meson momenta p_J in the nucleon rest frame are distributed over the range from 15 to 70 GeV/c with the maximum at $p_J \approx 40$ GeV/c [73]. Comparing the heavy ion results [1-4,6,7,72] with our calculations from Fig. 11 we also find reasonable agreement with $A + A$ data.

Furthermore, the nonperturbative QCD calculations [74] provide the $J/\Psi + N$ dissociation cross section of 4.4 ± 0.6 mb at J/Ψ meson momenta above 200 GeV, which is consistent with our results shown by Fig. 13.

XI. FUTURE PERSPECTIVES

There are a few problems that remain open and need further investigation.

In the present study we considered only OZI-allowed processes resulting in an endothermic inelastic reaction, where the total mass of the produced particles is larger than the initial mass $m_J + m_N$. These reactions provide the threshold behavior of the cross section. On the other hand, the OZI-suppressed reaction channels such as $J/\Psi + N \rightarrow N + n\pi$ with the number of the final pions from $n=1$ up to $m_J/m_\pi \approx 22$ are open even at $p_J=0$. These exothermic reactions, where the total final mass of the produced particles is less than the initial mass, provide a $1/p_J$ behavior of the $J/\Psi + N$ dissociation cross section.

For instance, the OZI-suppressed $J/\Psi + N \rightarrow N + \pi$ cross section was calculated by the ρ -meson-exchange model [75]. It was found that the cross section is negligibly small although it diverges at p_J close to zero, because it is exothermic. Furthermore, the ρ -meson-exchange model evaluates the $J/\Psi \rightarrow \rho + \pi$ vertex, which accounts only to tiny fraction, $\approx 1.27\%$, for the total hadronic decays of the J/Ψ meson. The multimeson OZI-suppressed reactions might play a non-negligible role for J/Ψ dissociation on a nucleon. Eventually, additional theoretical estimates are necessary in order to make a final conclusion about the possibility of $J/\Psi + N$ dissociation at low momenta.

Furthermore, we found a strong momentum dependence of the $J/\Psi + N$ dissociation cross section, as illustrated by Fig. 13. This momentum dependence of σ_{JN} might provide a partial explanation of the variation of the slope α from the

A^α dependence with the Feynman variable x_F . As was observed [71] in proton-nucleus collisions at beam energy of 800 GeV the extracted value for α is ≈ 0.9 at $x_F = 0.2$, while it decreases ≈ 0.8 at $x_F \approx 0.7$. The Feynman variable x_F is proportional to the J/Ψ meson momentum and one may naturally expect from the results shown in Fig. 13 that at large momenta p_J or equivalently large x_F the value for α extracted from the A^α dependence, should be smaller in comparison to small p_J . Now we can qualitatively predict that the slope α decreases with increasing x_F . However, a quantitative analysis needs further calculation.

An alternative is to reanalyze the experimental data on the A dependence of J/Ψ production from $p+A$ collisions and to evaluate the dissociation cross section as a function of the J/Ψ momentum. This will provide a crucial test of our calculations, since it can be directly compared to results shown in Fig. 13.

Furthermore, the ratio α_{JN} of the real to imaginary part of the $J/\Psi + N$ scattering amplitude at $t=0$, which is shown in Fig. 8, in principle can be measured using coherent J/Ψ production at diffractive minima [44]. Coherent J/Ψ photoproduction from nuclei seems to be an optimal way for such a measurement, however, one needs to perform further investigations in order to fix the sensitivity of the data to the sign and magnitude of the ratio α_{JN} .

Obviously, the form factor $F(t)$ at the $\gamma - J/\Psi$ vertex plays a key role for the comparison of our hadronic calculations with the data on $\gamma + N \rightarrow J/\Psi + N$ cross section. While this form factor is theoretically motivated at $t=0$ by the microscopic calculations given in Ref. [43], the evaluation of its t dependence still needs further studies. Our results shown in Fig. 12 should be considered as a phenomenological estimate for $F(t)$.

In addition, one can address the effect due to in-medium modification of the $J/\Psi + N$ dissociation cross section because of the strong changes of the D - and D^* -meson properties in nuclear matter [35,76]. As was found in Ref. [4] this modification plays a substantial role for J/Ψ dissociation on comovers. One might expect that the modification of the $J/\Psi + N$ dissociation cross section in nuclear matter might play no role for heavy ion collisions where the available J/Ψ momenta given in the nucleon rest frame are larger than $p_J > 13$ GeV, as was discussed above. However, to clarify the situation a detailed calculation of the in-medium modification of the $J/\Psi + N$ dissociation amplitude is necessary.

XII. SUMMARY

We have calculated the $J/\Psi + N$ dissociation cross section by a boson-exchange model, including D - and D^* -meson exchange and considering the $\Lambda_c + \bar{D}$ and $N + D + \bar{D}$ final states. We note that our results are in reasonable agreement with short-distance QCD calculations at high energies, while differing from them at low energies because of the $J/\Psi + N \rightarrow \Lambda_c + \bar{D}$ reaction channel explicitly included in our model.

To compare our results with the data on $\gamma + N \rightarrow J/\Psi + N$ cross section we introduced form factor at the $\gamma - J/\Psi$ vertex proposed in Ref. [43] and found good agreement with the photoproduction data.

Furthermore, we evaluated the real part of the $J/\Psi + N$ scattering amplitude at $t=0$, $f(0)$, using a dispersion relation and extrapolating our result for the dissociation cross section to infinite energy by the Regge theory [57,58]. Fixing the subtraction point for $\text{Re} f(0)$ at large energies with Regge theory, we were able to simultaneously saturate the $\text{Re} f(0)$ at zero momentum of J/Ψ meson given by the predictions for the J/Ψ mass shift in nuclear matter and for the $J/\Psi + N$ scattering length [48–53].

We estimate the elastic $J/\Psi + N \rightarrow J/\Psi + N$ cross section from our calculations and illustrate the compatibility of our results with the data on the total $\gamma + N \rightarrow J/\Psi + N$ cross section. It is important to note that the J/Ψ photoproduction data were used in our study mostly for illustrative purposes and do not influence the parameters of our calculations or the final results.

Finally, we predict the energy dependence of the $J/\Psi + N$ dissociation σ_{JN} and the elastic cross section over a large range of energies from 1 to 10^3 GeV. In contrast to the usual expectation of a constant dissociation cross section, we found that σ_{JN} varies strongly over the indicated range of energies. Our results are in agreement with the σ_{JN} evaluated phenomenologically from the experimental data on J/Ψ meson production in $\gamma + A$, $\rho + A$, and $A + A$ collisions.

ACKNOWLEDGMENTS

A.S. would like to acknowledge the warm hospitality and partial support of the CSSM during his visit. The discussions with E. Bratkovskaya, W. Cassing, C. Greiner, D. Kharzeev, and J. Speth are appreciated. This work was supported by the Australian Research Council and the Forschungszentrum Jülich.

[1] NA50 Collaboration, M. C. Abreu *et al.*, Phys. Lett. B **477**, 28 (2000).
 [2] W. Cassing, E. L. Bratkovskaya, and S. Juchem, nucl-th/0001024.
 [3] A. Capella, E. G. Ferreira, and A. B. Kaidalov, hep-ph/0002300.
 [4] A. Sibirtsev, K. Tsushima, K. Saito, and A. W. Thomas, nucl-th/9904015.
 [5] W. Cassing and E. L. Bratkovskaya, Nucl. Phys. A **623**, 570 (1997).

[6] W. Cassing and E. L. Bratkovskaya, Phys. Rep. **308**, 65 (1999).
 [7] N. Armesto, A. Capella, and E. G. Ferreira, Phys. Rev. C **59**, 395 (1999).
 [8] T. Matsui and H. Satz, Phys. Lett. B **178**, 416 (1986).
 [9] C. Spieles *et al.*, Phys. Rev. C **60**, 054901 (1999).
 [10] D. E. Kahana and S. H. Kahana, Prog. Part. Nucl. Phys. **42**, 269 (1999).
 [11] R. L. Anderson *et al.*, Phys. Rev. Lett. **38**, 263 (1977).
 [12] D. Kharzeev, C. Lourenço, M. Nardi, and H. Satz, Z. Phys. C

- 74**, 307 (1997).
- [13] K. Redlich, H. Satz, and G. M. Zinovjev, hep-ph/0003079.
- [14] S. G. Matinyan and B. Müller, Phys. Rev. C **58**, 2994 (1998).
- [15] B. Müller, Nucl. Phys. **A661**, 272 (1999).
- [16] K. L. Haglin, Phys. Rev. C **61**, 031902(R) (2000).
- [17] K. Haglin and C. Gale, nucl-th/0002029.
- [18] C. Y. Wong, E. S. Swanson, and T. Barnes, nucl-th/0002034.
- [19] T. Barnes, E. S. Swanson, and C. Y. Wong, nucl-th/0006012.
- [20] Z. Lin and C. M. Ko, nucl-th/9912046.
- [21] Z. Lin, C. M. Ko, and B. Zhang, Phys. Rev. C **61**, 024904 (2000).
- [22] A. Sibirtsev and W. Cassing, nucl-th/9802019.
- [23] A. Sibirtsev, Phys. Lett. B **359**, 29 (1995).
- [24] A. D. Martin, Nucl. Phys. **B179**, 33 (1981).
- [25] J. M. Laget, Phys. Lett. B **259**, 24 (1991).
- [26] A. Sibirtsev and W. Cassing, Nucl. Phys. **A641**, 476 (1998).
- [27] F. S. Navarra and M. Nielsen, Phys. Lett. B **443**, 285 (1998).
- [28] R. A. Adelseck and B. Saghai, Phys. Rev. C **42**, 108 (1990).
- [29] T. Feuster and U. Mosel, Phys. Rev. C **58**, 457 (1998).
- [30] R. Machleid, K. Holinde, and C. Elster, Phys. Rep. **149**, 1 (1987).
- [31] L. G. Landsberg, Phys. Rep. **128**, 301 (1985).
- [32] R. Machleid, Adv. Nucl. Phys. **19**, 189 (1989).
- [33] D. Lohse, J. W. Durso, K. Holinde, and J. Speth, Nucl. Phys. **A516**, 533 (1990).
- [34] V. B. Berestetsky and I. Ya. Pomeranchuk, Nucl. Phys. **22**, 629 (1961).
- [35] A. Sibirtsev, K. Tsushima, and A. W. Thomas, Eur. Phys. J. A **6**, 351 (1999).
- [36] A. Sibirtsev, Nucl. Phys. A (to be published).
- [37] D. Kharzeev and H. Satz, Phys. Lett. B **334**, 155 (1994).
- [38] V. Shevchenko and P. Volkovitsky, Phys. At. Nucl. **59**, 1659 (1996).
- [39] D. Kharzeev, H. Satz, A. Syamtomov, and G. Zinovjev, Eur. Phys. J. C **9**, 459 (1999).
- [40] M. Peskin, Nucl. Phys. **B156**, 365 (1979).
- [41] G. Bhanot and M. Peskin, Nucl. Phys. **B156**, 391 (1979).
- [42] A. Martin, R. Roberts, and W. Stirling, Int. J. Mod. Phys. A **10**, 2885 (1995).
- [43] J. Hüfner and B. Z. Kopeliovich, Phys. Lett. B **426**, 154 (1998).
- [44] T. H. Bauer, R. D. Spital, D. R. Yennie, and F. M. Pipkin, Rev. Mod. Phys. **50**, 261 (1978).
- [45] L. A. Kondratyuk, A. Sibirtsev, W. Cassing, Ye. S. Golubeva, and M. Effenberger, Phys. Rev. C **58**, 1078 (1998).
- [46] Y. Nambu and J. J. Sakurai, Phys. Rev. Lett. **8**, 79 (1962).
- [47] A. Donnachie and P. V. Landshoff, Phys. Lett. B **296**, 227 (1992).
- [48] M. Luke, A. V. Manohar, and M. J. Savage, Phys. Lett. B **288**, 355 (1992).
- [49] G. F. de Teramond, R. Espinoza, and M. Ortega-Rodriguez, Phys. Rev. D **58**, 034012 (1998).
- [50] S. J. Brodsky and G. A. Miller, Phys. Lett. B **412**, 125 (1997).
- [51] F. Klingl, S. Kim, S. H. Lee, P. Morath, and W. Weise, Phys. Rev. Lett. **82**, 3396 (1999); **83**, 4224 (1999).
- [52] A. Hayashigaki, Prog. Theor. Phys. **101**, 923 (1999).
- [53] S. Kim and S. H. Lee, nucl-th/0002002.
- [54] U. Camerini *et al.*, Phys. Rev. Lett. **35**, 483 (1975).
- [55] B. Gittelman *et al.*, Phys. Rev. Lett. **35**, 1616 (1975).
- [56] M. Binkley *et al.*, Phys. Rev. Lett. **48**, 73 (1982).
- [57] A. Donnachie and P. V. Landshoff, Phys. Lett. B **470**, 243 (1999).
- [58] A. Donnachie and P. V. Landshoff, Phys. Lett. B **437**, 408 (1998).
- [59] A. Donnachie and P. V. Landshoff, hep-ph/9912312.
- [60] H1 Collaboration, C. Adloff *et al.*, hep-ex/0003020.
- [61] ZEUS HERA Collaboration, J. Breitweg *et al.*, Eur. Phys. J. C **12**, 35 (2000).
- [62] ZEUS HERA Collaboration, J. Breitweg *et al.*, hep-ex/9910038.
- [63] H1 Collaboration, S. Aid *et al.*, Nucl. Phys. **B472**, 3 (1996).
- [64] ZEUS HERA Collaboration, J. Breitweg *et al.*, Z. Phys. C **75**, 215 (1997).
- [65] A. B. Kaidalov, L. A. Ponomarev, and K. A. Ter-Martirosian, Yad. Fiz. **44**, 722 (1986) [Sov. J. Nucl. Phys. **44**, 468 (1986)].
- [66] A. Sibirtsev, Yad. Fiz. **55**, 259 (1992) [Sov. J. Nucl. Phys. **55**, 145 (1992)].
- [67] L. A. Kondratyuk *et al.*, Phys. Rev. C **48**, 2491 (1993).
- [68] W. Lenz, Z. Phys. **56**, 778 (1929).
- [69] C. D. Dover, J. Hüfner, and R. H. Lemmer, Ann. Phys. **66**, 248 (1971).
- [70] J. D. Bjorken and S. D. Drell, *Relativistic Quantum Fields* (McGraw-Hill, New York, 1965).
- [71] D. M. Alde *et al.*, Phys. Rev. Lett. **66**, 133 (1991).
- [72] R. Vogt, Phys. Rep. **310**, 197 (1999).
- [73] W. Cassing (private communication).
- [74] H. G. Dosch, F. S. Navarra, M. Nielsen, and M. Rueter, Phys. Lett. B **466**, 363 (1999).
- [75] A. Sibirtsev and K. Tsushima, nucl-th/9810029.
- [76] K. Tsushima, D. H. Lu, A. W. Thomas, K. Saito, and R. H. Landau, Phys. Rev. C **59**, 2824 (1999).